

Miniaturized Lab-on-a-Disc (miniLOAD)

Nick R. Glass, Richie J. Shilton, Peggy P. Y. Chan, James R. Friend,*
and Leslie Y. Yeo*

A miniaturized centrifugal microfluidic platform for lab-on-a-chip applications is presented. Unlike its macroscopic Lab-on-a-CD counterpart, the miniature Lab-on-a-Disc (miniLOAD) device does not require moving parts to drive rotation of the disc, is inexpensive, disposable, and significantly smaller, comprising a 10-mm-diameter SU-8 disc fabricated through two-step photolithography. The disc is driven to rotate using surface acoustic wave irradiation incident upon a fluid coupling layer from a pair of offset, opposing single-phase unidirectional transducers patterned on a lithium niobate substrate. The irradiation causes azimuthally oriented acoustic streaming with sufficient intensity to rotate the disc at several thousand revolutions per minute. In this first proof-of-concept, the capability of the miniLOAD platform to drive capillary-based valving and mixing in microfluidic structures on a disc similar to much larger Lab-on-a-CD devices is shown. In addition, the ability to concentrate aqueous particle suspensions at radial positions in a channel in the disc dependent on the particles' size is demonstrated. To the best of our knowledge, the miniLOAD concept is the first centrifugal microfluidic platform small enough to be self-contained in a handheld device.

1. Introduction

Miniaturization of existing large-scale laboratory technologies and processes, with the aim of producing inexpensive portable devices that duplicate the full range of laboratory-based chemical and biological assays, has been a key goal of microfluidics from its conception.^[1] Such lab-on-a-chip devices have many advantages beyond portability. Diagnostics, for

example, can be conducted with enhanced sensitivity and selectivity at a fraction of the cost and time associated with conventional assays because of the far smaller (nano to picoliter) analyte volumes. Moreover, advances in micro- and nanofabrication techniques not only allow these miniaturized devices to be inexpensively manufactured by exploiting economies of scale, but also facilitate automated parallelization and the possibility of on-time repetitive sampling. In addition, reaction timescales can be drastically reduced and enhanced interfacial transport can be achieved through the large surface-area-to-volume ratios available at such small scales. The infrastructure and transport needed for laboratory diagnostic facilities can be eliminated in favor of point-of-care devices, thus eliminating the risk of contamination and sample tracking problems.

One of the most severe technical obstacles encountered in realizing truly miniaturized and portable lab-on-a-chip devices, however, is the inability to drive microfluidic processes on the chip itself. For example, large and cumbersome capillary pumps or power supplies external to the chip-scale device are often required—quite the antithesis of microfluidic philosophy.^[2] One attempt to circumvent this limitation

N. R. Glass,^[+] R. J. Shilton,^[+] Dr. P. P. Y. Chan,
Prof. J. R. Friend, Prof. L. Y. Yeo
Micro/Nanophysics Research Laboratory
School of Electrical & Computer Engineering
RMIT University
Melbourne, VIC 3000, Australia
E-mail: james.friend@rmit.edu.au; leslie.yeo@rmit.edu.au



N. R. Glass, R. J. Shilton
Micro/Nanophysics Research Laboratory
Monash University
Clayton, VIC 3800, Australia
[+] N.R.G. and R.J.S. contributed equally to this work.

DOI: 10.1002/sml.201102282

is the Lab-on-a-CD platform,^[3–5] in which fluidic operations are carried out in channels fabricated on a compact disc (CD) or similar structure, and driven by the bulk rotation of the entire CD using a laboratory-scale rotational motor akin to a CD player. The ingenuity in inexpensively carrying out a variety of functions such as valving, metering, pumping, and mixing^[3,4,6–9] is evident in the widespread attention the technology has received to date.

The initial Lab-on-a-CD concept has since advanced to commercially available devices serving a range of chemical and biological applications. A number of researchers have independently demonstrated simple and effective blood plasma separation.^[10–12] Single-step on-chip blood-based diagnostics costing as little as US\$10 have been developed from the Lab-on-a-CD platform.^[13] Cho et al.^[14] showed extraction of both hepatitis B virus and *Escherichia coli* DNA from blood in a one-step process. Preconcentration of trace metals was also demonstrated by Lafleur et al.^[15] as a complementary route to another detection process. These developments represent advances toward realistic and widespread use of lab-on-a-chip technology, yet the size of the CD itself, usually equivalent to that of a commercial video disc at around 100 mm in diameter or greater, and the necessity of a CD player system or laboratory-scale rotational motor, are drawbacks to applying the technology for portable, handheld, field use.

Various fundamental actuation concepts underlying the Lab-on-a-CD technology have been explored, such as the deceptively simple capillary valve,^[3,16,17] in addition to a broad variety of methods for fabrication of the CD structures.^[18] Novel actuation methods based on siphoning,^[4] out-of-plane valves,^[11] vacuum-based liquid removal,^[19] pneumatic pumping,^[20] and even liquid recirculation in channels^[21] have also been developed. In addition, various other laboratory processes have been explored, such as precise liquid aliquoting^[19] and mixing enhancement.^[6]

Herein, we report the development of the miniaturized Lab-on-a-Disc (miniLOAD) concept—a complete on-chip version of the Lab-on-a-CD platform which does not involve any mechanically moving parts. The discs we employ, on which 150–250- μm -wide microfluidic channels are patterned, are one order of magnitude smaller—10 mm in diameter in the concept tested here, although this can be scaled down further—and their rotation is driven by surface acoustic waves (SAWs) coupled into a fluid layer on which the disc is placed.^[22] As seen in **Figure 1a** and **b**, as well as the movie showing the operation of the Lab-on-a-Disc platform (see Supporting Information), the SAW actuation device and disc are together smaller than a typical USB flash drive, the entire system including a camera-battery-powered driver circuit and being small enough to sit in the palm of one's hand. The reduced disc and device sizes as well as the integration of the device with the power supplies not only allow further miniaturization of the devices, particularly for versatile portable or field use, but also facilitate relatively small working volumes of fluids, typically on the order of 100 nL, particularly attractive when expensive reagents are used or when increased sensitivity is desired. Moreover, the discs, mass fabricated out of SU-8 photoresist using two-step photolithography in this

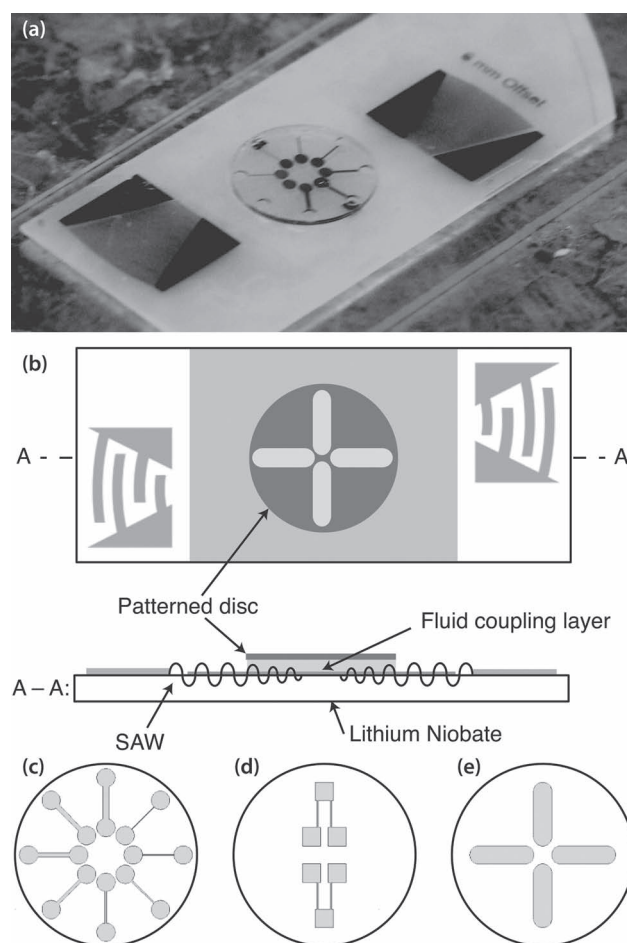


Figure 1. a) Image and b) schematic of the miniLOAD device, which comprises a pair of offset elliptically focusing single-phase unidirectional transducers (SPUDTs) patterned onto a Teflon AF-coated lithium niobate substrate, a water drop serving as a fluid coupling layer pipetted onto the device and confined within a masked hydrophilic region, and a thin SU-8 disc placed on top of the coupling layer. The disc has microfluidic structures patterned into its top surface to demonstrate c) capillary valving, d) mixing, and e) particle concentration. A movie showing the device in operation is provided in the Supporting Information.

study, can also be made from a variety of inexpensive materials via hot embossing with far less material required for each disposable disc compared to the Lab-on-a-CD, thus representing an inexpensive alternative. The SAW device itself is also inexpensive, robust, and reliable as a consequence of decades of development of such technology for the telecommunications industry, and is reusable.^[23]

2. Results and Discussion

2.1. SAW Microcentrifugation

The rotational actuation technology of the miniLOAD platform has its origins in the ability of the SAW,^[24] nanometer-amplitude Rayleigh electroelastic waves generated on a piezoelectric substrate, to drive microcentrifugation in a sessile fluid drop through symmetry breaking of the planar

wave such that the acoustic radiation is imparted laterally on only part of the drop.^[25] The resultant rotation within the drop, an azimuthal form of acoustic streaming, is rapid, typically on the order of several centimeters per second, and has been demonstrated for effective mixing^[25] as well as particle concentration/separation and sorting.^[25] In addition, we have also demonstrated the ability for the SAW to be coupled through a fluid layer into a superstrate on which drops can be manipulated,^[23] thereby forming the basis for more advanced droplet microfluidic operations and applications.^[26,27]

Together, the SAW microcentrifugation and superstrate concepts have led to the development of an on-chip centrifugal micromotor, where the azimuthal streaming in the fluid coupling layer on which a thin disc is placed is capable of rotating it up to almost 10 000 rpm.^[22] However, for 10-mm-diameter, 300- μm -thick SU-8 discs on which microchannels are patterned, rotation speeds of up to around 1500 rpm can be generated. The associated radial acceleration of approximately 10^2 m s^{-2} at the outer regions of the disc can be exploited to drive a number of microfluidic processes—but in a much smaller disposable device and without the need of additional moving parts, therefore eliminating potential wear problems and offering the simplicity of solid-state actuation. It is further possible to scale down the miniLOAD technology since it has already been shown that discs down to 200 μm in diameter can be rotated at high speeds.^[22] Initial proof is provided of the miniLOAD concept and its ability to drive capillary valving and mixing as representative microfluidic operations similar to those first shown in the original Lab-on-a-CD concept.^[3] In addition, concentration of particles in aqueous suspension is demonstrated, with the unique ability to partition particles at specific locations along the radial axis depending on their size.

2.2. Fabrication and Method

The SAW devices were fabricated using standard microfabrication techniques. Briefly, 127.68° *Y*-axis rotated, *X*-axis propagating lithium niobate wafers (University Wafer, South Boston, MA, USA) were cleaned by successive sonication in acetone, isopropanol, and water, followed by forced nitrogen drying. The wafers were then cleaned in a fresh piranha solution. Aluminum single-phase unidirectional transducer (SPUDT) electrodes with an elliptical focus were subsequently fabricated on the substrate using conventional photolithography and etching techniques,^[25] as depicted in Figure 1a and b. The finger width and spacing of the focused SPUDTs were designed for resonance at 30 MHz, and each device on the wafer comprised an opposing SPUDT pair laterally offset by 4.5 mm to form mutually opposing acoustic radiation into the coupling layer symmetric about its center to drive acoustic streaming and consequent azimuthal fluid motion;^[22] the direction of disc rotation can simply be reversed by switching the placement of the interdigital transducers such that the acoustic radiation enters from the alternate ends of the drop. The devices were then diced from the wafer using a diamond scribe (DTX, Dynatex International, Santa Rosa, CA, USA). The pair of SPUDT electrodes and

the 10-mm-diameter circular region were masked with dicing tape. A Teflon AF (DuPont, Wilmington, DE, USA) layer was subsequently deposited onto the device via spin-coating at 500 and 4000 rpm for 10 and 30 s, respectively, followed by the removal of the masks. The device was next baked at 80 °C for 1 h, thereby crystallizing the Teflon AF layer and forming a strongly hydrophobic surface save for the SPUDTs and the bare hydrophilic circular region where the fluid coupling drop and disc is to be placed. Wave reflections at the device's edges were reduced through absorption by an energy-dissipating polymer (First Contact Polymer, Photonic Cleaning Technologies, Platteville, WI, USA) deposited on the edges of the SAW device.

The discs were fabricated from SU-8 photoresist (MicroChem Corp., Newton, MA, USA) using two-step photolithography. To prevent adhesion of the SU-8 to its Si substrate and facilitate removal of the fabricated SU-8 discs, wafers were treated with trichloro(1*H*,1*H*,2*H*,3*H*-perfluorooctyl)silane (Sigma-Aldrich Pty. Ltd., Castle Hill, NSW, Australia) prior to fabrication. This was achieved through vapor deposition in a vacuum desiccator for approximately 30 min. An initial layer of SU-8 2035 was then spun onto the wafer to achieve a nominal thickness of 100 μm , followed by UV exposure to form the base of the discs. A second layer of SU-8 2075 with an approximate thickness of 200 μm was spun and subsequently baked to form the disc with the various microchannel patterns shown in Figure 1c–e with the aid of a mask; each channel had a depth of 200 μm . We note that the SU-8 film slightly receded leading to regions of nonuniform thickness around the edges of the substrate wafer; discs in these regions were discarded. Finally, the SU-8 was developed and the discs were mechanically removed.

For the valving experiments, the disc was loaded with liquid mixtures of approximately 1:9 parts glycerol to water (glycerol was used to reduce evaporation while preparing the sample) before the disc was placed atop a small water drop pipetted onto the hydrophilic circular region of the SAW device. All other experiments employed water as the working fluid, either mixed with food dye for the mixing tests or dispersed with fluorescent microparticles (Duke Scientific, Fremont, CA, USA) ranging from 200 nm to 31 μm in diameter for the particle concentration studies. Fluids were loaded into the channels on the disc using pipettes—given the availability of automatic pipetting technology, we envisage this would be a simple and straightforward way for fluid transfer in and out of the discs in practice. To generate the SAW signal at both ends of the opposing SPUDTs, an oscillating electrical signal from a signal generator (SML-01, Rohde & Schwarz, North Ryde, NSW, Australia) was passed through an amplifier (10W1000C, Amplifier Research, Souderton, PA, USA) and connected to each SPUDT in parallel through a pair of SMA cables and custom-made electrical contact probes. The average unloaded SAW peak amplitudes were measured with the aid of a laser Doppler vibrometer (MSA-400, Polytec GmbH, Waldbronn, Germany).

Experimental images, on the other hand, were acquired using a variety of microscopes and cameras. High-speed disc rotation was captured by a digital camera (iSpeed, Olympus, Tokyo, Japan) attached to a long-working-distance lens

(Infinivar CFM-2/S, Infinity, Boulder, CO, USA). The subsequent angles were then measured in ImageJ (National Institutes of Health, Bethesda, MD, USA) and the velocities calculated from these data. Images for the valve actuation were captured on a small USB camera (AM7023 Dino-Eye, AnMo Electronics Corp., Taipei, Taiwan), while mixing and particle concentration pictures were taken on a high-resolution camera (EOS 550D SLR, Canon, Tokyo, Japan). Fluorescence illumination of the particles in suspension was achieved using a simple 40 W black light (Nelson Industries, Melbourne, VIC, Australia).

2.3. Device Characterization

Using unloaded discs, the devices were first characterized to determine the appropriate volume of water to be used as the coupling fluid. **Figure 2** shows the disc rotation speed to be unaffected by the volume of fluid couplant used for a given input power, consistent with previous results obtained for discs made from different materials and of different sizes.^[22] We observed, however, that disc precession became increasingly prevalent as the fluid volume was increased, which led to a larger variance in the data set. As such, the remainder of the experiments was carried out with a smaller fluid volume (75 μL). In addition, we also characterized the devices to determine the disc rotation speed as a function of the input power, measured through the surface displacement of the substrate as the SAW traverses. A typical response curve can be seen in **Figure 2**, in which we observe the rotation speed to increase up to approximately 1400 ± 30 rpm at a surface displacement of about 1.7 nm. Beyond this level, the precession of the disc prevented further increases in the disc rotation speed. Droplets were expelled from the meniscus of the fluid coupling layer at these large displacement amplitudes due to

the large centrifugal stresses present that drove a capillary instability along the meniscus. Consequently, the experiments were conducted with surface displacements below 2 nm to ensure stability of the disc's rotation and the fluid coupling layer.

Although each of these experiments was conducted within open channels on the discs' surface, evaporation of the small fluid volumes in the channels and reservoirs was negligible within the short time periods that each process was performed. To further mitigate evaporative effects in the case of longer running processes, these processes could alternatively be performed in closed channels or, if necessary, carried out on heat sinks or Peltier coolers to control the device temperature. Closed channel functionality will be explored further in subsequent studies.

2.4. Microfluidics

2.4.1. Capillary Valving

Simple capillary valve operations were demonstrated on the miniLOAD platform by designing circular inlet and outlet reservoirs connected by microchannels of different widths (**Figure 1c**). In general, fluid flows easily into the channel from the source reservoir, but not from the channel into the outer reservoir due to the restoring capillary stress imposed by the meniscus curvature at the channel aperture. The "channel valve" therefore remains "closed" (**Figure 3a**) until there is sufficient radial acceleration from the disc rotation to overcome the capillary force retarding the meniscus, thus allowing the fluid to pass into the outer reservoir (**Figure 3b-d**). A balance of the two dominant and opposing forces that govern the rotational behavior gives^[16]

$$\rho\omega_c^2\bar{r}\Delta r = \frac{4\gamma}{D_h}a + b \quad (1)$$

where ρ is the liquid density, ω_c the critical burst frequency, that is, the disc angular rotation speed at which the capillary valve first "opens", \bar{r} the center of mass of the fluid in the channel, Δr the distance from the inlet to the liquid front, γ the surface tension of the liquid, and D_h the channel hydraulic diameter. a is a nondimensional correction factor dependent on the wetting properties and the geometry of the outlet reservoir that accounts for the nonspherical meniscus curvature, and b is the pressure required to initiate the flow. The plot in **Figure 3** shows reasonable agreement of the experimental data with Equation 1, with $a = 0.275$ and $b = -236$ Pa calculated through least-squares fitting of the data to the equation. From Equation 1, the maximum channel dimension beyond which the fluid cannot be restricted at the juncture between the channel and the output reservoir, even in the absence of disc rotation ($\omega_c = 0$), is approximately $560 \mu\text{m}$. Since the capillary stress scales inversely to the channel dimension, faster rotation is therefore required to "open" the smaller channel valves, consistent with the results shown in **Figure 3e**. While the results were repeatable and consistent across multiple discs and independent devices, we note that valves with channel dimensions below $100 \mu\text{m}$ operated less reliably. In

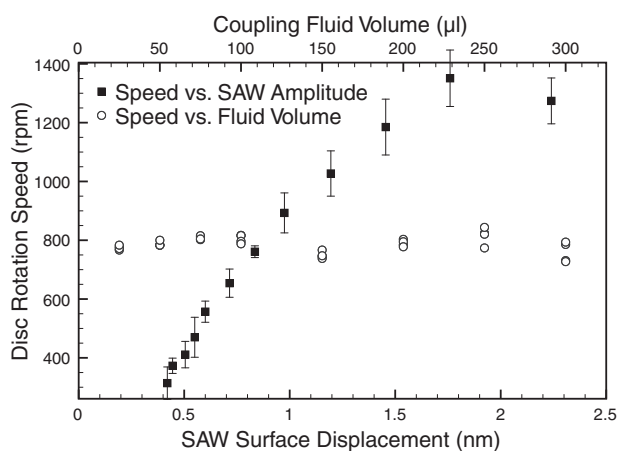


Figure 2. The disc rotation speed was roughly proportional to the surface displacement of the SAW substrate from about 0.5 to 1.7 nm in amplitude; beyond this value, the rotation speed remained fairly constant due to disc precession and other effects. These data were taken for a fixed volume of fluid couplant (75 μL ; squares). However, the rotation speed was not significantly affected by the volume of the fluid couplant used with the 10 mm disc when using a fixed surface displacement (≈ 1 nm; circles).

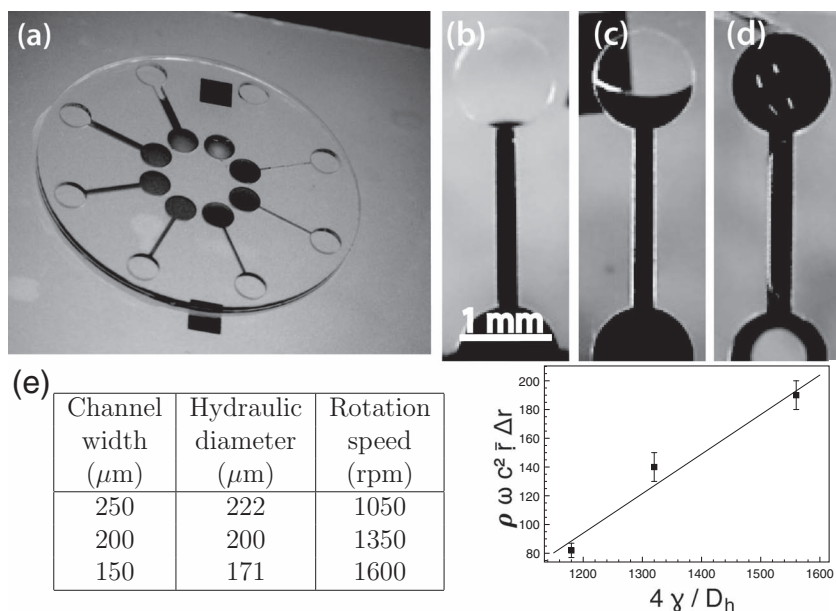


Figure 3. a) Capillary valves in the miniLOAD device consisting of inlet and outlet reservoirs connected by 200- μm -deep channels of different widths in the “closed” position prior to disc rotation. b–d) “Opening” of a typical 200- μm -wide capillary valve upon disc rotation at approximately 1350 rpm for around 20 s; the top of the images are radial locations further from the disc center. The interval between the successive images in (b–d) is approximately 10 s. e) The rotation speed required to “open” a capillary valve of a channel connected to a reservoir is inversely proportional to the width of the channel; the adjacent plot shows good agreement with the dominant force balance given by Equation 1. The error bars in the plot indicate the standard error over five runs across different discs from the same fabrication batch.

these cases, the critical burst frequencies exceeded 2100 rpm, consistent with that predicted by Equation 1 and well above the disc speeds reported in Figure 2 where excessive disc precession was noticed. Smaller functional valves can nevertheless be achieved by optimizing the device to reduce the level of disc precession or by modifying the geometry and surface properties of the channel valves.

2.4.2. Mixing

We now explore the feasibility of mixing two fluids using the miniLOAD device. By opening the capillary valves formed by two channels connecting separate inlet reservoirs into an outlet reservoir (Figure 1d) upon rotation, two fluid species housed in the inlet reservoirs can be driven into the outlet reservoir and mixed. We demonstrate this concept by initially loading the reservoirs with a liquid, one containing approximately 50 $\mu\text{L mL}^{-1}$ of black food dye (Queen Fine Foods, Alderley, QLD, Australia), the other simply water. In the absence of rotation, capillary filling of the channels occurred as expected, and formed a blocking meniscus at the end of each channel at the entry into the outlet reservoir, as shown in Figure 4a. Upon disc rotation at approximately 1000 rpm, both fluids then entered the chamber (Figure 4b) and uniformly mixed into a homogeneous solution upon further rotation (Figure 4c).

Given that a pixel intensity analysis is a common way to show mixing efficiency between two solutions,^[25,28] we

first converted the frames into grayscale images. A 200 \times 200 pixel area was analyzed for each of the inlet reservoirs and the single outlet reservoir. Figure 4d shows the normalized pixel counts and intensities in the reservoirs prior to and after rotation (and hence mixing). The pixel intensity was normalized such that bright pixels and dark pixels had a median intensity value of 1 and 0, respectively. The pixel count was also normalized so that the area of each distribution was equal to unity. In addition, the inset of Figure 4d shows the standard deviation of the normalized pixel intensities in the output reservoir after it filled, and indicates the mixing reaching completion after around 4 s of rotation at a speed of approximately 1000 rpm; the standard deviations were normalized so that the initial and final values in the inset of Figure 4d were 1 and 0, respectively. Both Figure 4d and its inset therefore clearly show that the two fluids proceeded to mix to form a solution with an intensity bracketed by the intensity values of the two inlet reservoirs. Over approximately 15 s of rotation, the outlet chamber filled with fluid from both inlet reservoirs and a homogeneous intensity roughly the average of the source fluids’ intensities was generated in the outlet reservoir in just 4 s after disc rotation commenced.

2.4.3. Particle Concentration

The centrifugal forces generated by the miniLOAD platform can also be exploited to drive particle concentration and separation within chambers fabricated on the disc. Such operations can be useful, for example, for enhancing on-chip detection to circumvent limitations in the sensitivity that currently plague typical sensing technology.^[2] By loading the chambers illustrated in Figure 1e, each of length 3.5 mm and width 1 mm, with a dispersion of 5 μm fluorescent particles, we were able to concentrate particles at the center of the outer region of the chamber by spinning up the disc to approximately 1400 rpm. Figure 5a and b show the uniform mixture of 5 μm particles in the chamber before and at the start of rotation, respectively, whereas Figure 5c shows the concentration of the particles during rotation. Upon termination of the disc rotation after 10 s, we observe that the particles remain aggregated roughly in the center of each chamber due to van der Waals attraction. As such, the particle cluster can be readily and simply extracted from the chamber using a pipette, the operation of which can be automated with currently available technology.

We also examined the effect of varying the particle size by placing suspensions of 200 nm, 500 nm, 1 μm , 5 μm , and 31 μm separately in each individual chamber, followed by their collective rotation at the same speed over a similar

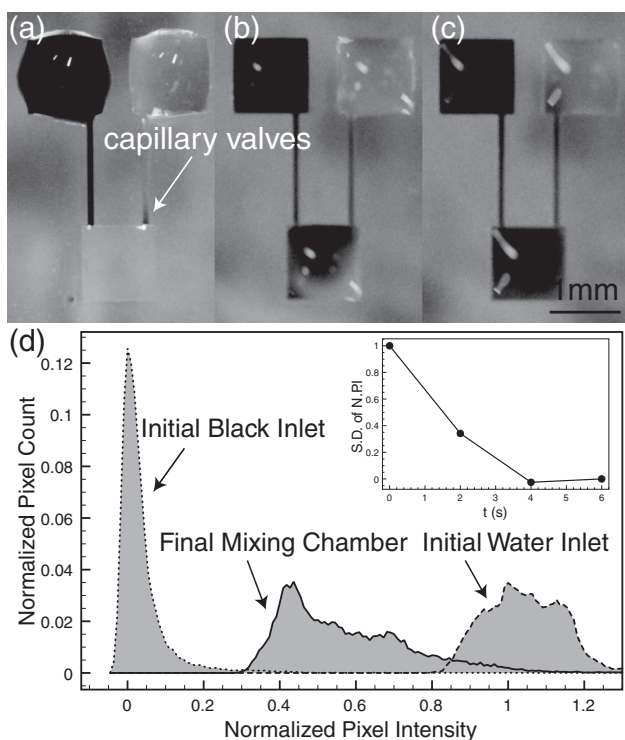


Figure 4. Demonstration of mixing on the miniLOAD platform. Water is placed in a pair of inlet reservoirs, one of which is also mixed with black food dye at a ratio of approximately 1:50. The inlet reservoirs are connected by channels oriented radially outwards that issue into a single outlet port. a) Upon deposition of the fluid into the inlet reservoir, the channels are observed to fill almost spontaneously. b) During disc rotation over approximately 15 s at around 1000 rpm, the capillary valves “open” and the outlet reservoir fills with the two fluids. c) After further rotation, the fluids are seen to be completely mixed. d) For quantification, a pixel intensity analysis was carried out on a 200×200 pixel region of the grayscale images, normalized against pixel intensity such that bright pixels and dark pixels had an intensity value of 1 and 0, respectively. The pixel count was also normalized such that the total pixel count under each distribution sums to 1. The pixel intensity histograms for the inlet reservoirs containing water with and without the black dye prior to disc rotation are given by the dotted and dashed lines, respectively, whereas the corresponding histogram for the outlet reservoir is represented by the solid line and shows the emergence of an intermediate gray population between the two initial states as they mix. The inset comprises a plot of the standard deviation in the normalized pixel intensity of the outlet reservoir as a function of time t , and shows that the mixing completes in approximately 4 s of rotation after the chamber was initially filled with the two fluids (when $t = 0$ s), as ascertained when the standard deviation approaches its minimum value.

time interval. The normalized pixel intensity plot in Figure 5e quantitatively shows the location along the centerline of the chamber where the different sized particles concentrate. We observed the four larger-particle species to concentrate in clusters at different locations along the centerline of the chamber, as observed by the peaks in their fluorescence intensity distributions shown in Figure 5e. Smaller particles are observed to aggregate at radial positions in the chamber further from the center of the disc.

With the exception of the smallest (200 nm) particles, which failed to concentrate and remained dispersed

throughout the entire chamber, thus suggesting the existence of a cutoff in the particle size, the radial position r at which the particles concentrate along the centerline of the chamber roughly scales linearly with the particle size a , as shown in Figure 5f. Clearly, the underlying principles governing conventional differential or density-gradient centrifugation do not apply in the present case, given the markedly different geometry and scales involved. Further, the system is considerably more complex given the existence of additional forces acting on the particles beyond centrifugal force and fluid drag. These additional forces are imposed by the acoustic energy transmitted into the disc via the fluid coupling layer.^[23] Traveling waves along the disc are expected to impart a direct acoustic force on a particle that scales as a^6 whereas standing waves, generated in the fluid due to strong reflections at the boundaries of the chamber and the disc, give rise to a similar force that scales as a^3 .^[29] Further, it is also known that Coriolis forces can be significant at these scales.^[30]

Here, we provide simple scaling arguments to speculate why a linear size-dependent separation is observed in Figure 5f. Given the small micrometer order particle dimension, it is likely that the fluid drag acting on the particles, which scales linearly with respect to a regardless of whether the flow in the chamber is induced by the disc rotation or by acoustic streaming^[24] as a consequence of the acoustic forces transmitted into the disc, dominates over any direct acoustic forces acting on the particle. A mechanism by which particles in a rotational microfluidic system are likely to concentrate into vortical clusters, based on diffusional cross-streamline transport arising as a consequence of shear gradients, has been discussed elsewhere.^[25] For approximate shear rates $\dot{\gamma} \approx \partial v_\theta / \partial r \approx 10^3 \text{ s}^{-1}$, the diffusion time for particles of size a to concentrate into clusters of size R is $(R/a)^2 / \gamma\phi$, which is on the order of 0.1 s for a local particle volume fraction ϕ close to 1;^[31] here, v_θ is the azimuthal velocity. As such, it is not unreasonable to assume that the concentration of the particles into clusters with dimension R occurs on a timescale much faster than the radial separation shown in Figure 5e. A dominant balance between the centrifugal force acting on the cluster of concentrated particles of dimension R , which serves to drive the entire cluster towards the disc periphery (large r), and the drag imposed on the cluster that retards this motion

$$\rho_p R^3 \omega^2 r \approx \mu v_r R \quad (2)$$

is then expected to lead to the selection of a specific equilibrium position r along the centerline of the chamber for a cluster of particles with size a . In the above, ρ_p is the particle density, ω the disc rotation speed, v_r the radial velocity of the fluid in the chamber, and μ the fluid viscosity.

The cluster size R is nevertheless dependent on a . Assuming that the particles concentrate into a planar spot, the growth rate of the cluster is given by the effective cross-streamline particle diffusion rate, which can be obtained by considering multiparticle interactions with scatter lengths comparable to the particle dimension:^[31]

$$\frac{d(R^2)}{dt} = 2\pi R \frac{dR}{dt} \approx \dot{\gamma} a^2 \phi \quad (3)$$

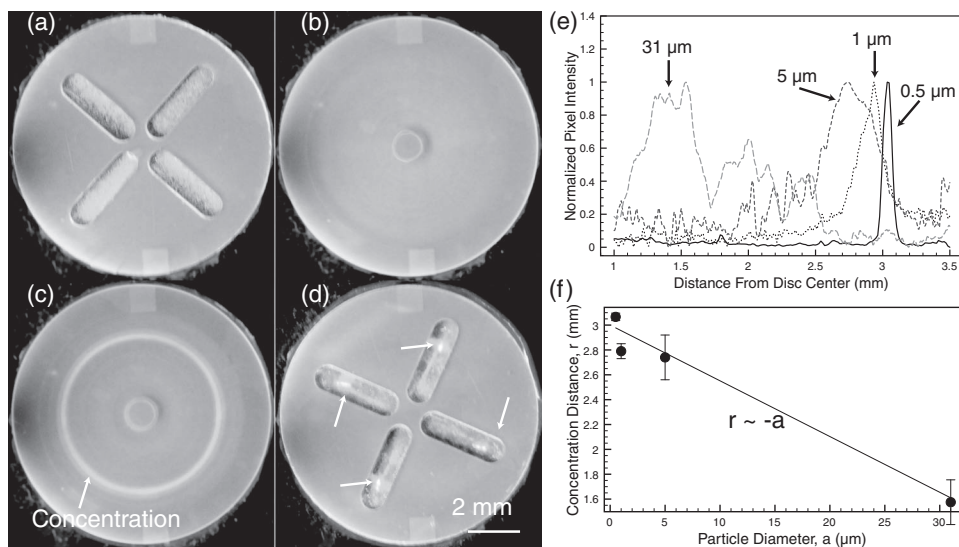


Figure 5. a) Aqueous suspensions of 5 μm fluorescent particles loaded into four separate chambers on the disc. b) As the disc is rotated at approximately 1400 rpm, we observe the particles to c) concentrate, as indicated by the arrow. d) Upon relaxation of the disc rotation, the 5 μm particles remain concentrated in roughly the center of each chamber, as indicated by the arrows. To further examine the effect of particle size on their concentration, individual suspensions of different particle sizes (200 nm, 500 nm, 1 μm , 5 μm , and 31 μm) were placed separately in each chamber. With rotation of the chamber at the same speed and over the same time interval, all the particle species except the smallest 200 nm particles collect at different locations along the centerline in each chamber, as shown by e) the distributions in their fluorescence intensity (as captured by the grayscale pixel intensity). The pixel intensity is normalized such that the brightest pixels due to the particle fluorescence have a value of 1 and the darkest pixels in the absence of particles have an intensity of 0; the data are averaged from a sequence of concentration images over four successive runs. It can therefore be seen that smaller particles concentrate more effectively (as observed by the narrower and sharper peaks in their distribution) at centerline positions further away from the center of the disc, as depicted by f) the approximate linear relationship between the radial centerline position r at which clusters comprising particles of size a concentrate.

where t denotes the time. Given that the azimuthal Reynolds number $\text{Re}_\theta \equiv \rho\omega D^2/\mu \approx 10^3$, where D represents the disc dimension, an inertia-dominant azimuthal flow can be assumed. For an irrotational vortex undergoing potential flow, $v_\theta \approx 1/r$, from which it follows that $\dot{\gamma} \approx 1/r^2$ and hence we find from Equation 3

$$R \approx \frac{a}{r} \quad (4)$$

Qualitatively, this agrees with our experiments in which we observe the concentration to be apparently more effective for smaller particles, with the particles more tightly aggregating into a smaller region, evident by the sharper and narrower intensity peaks in Figure 5e.

It is likely, however, that the longitudinal flow in the chamber in the r direction is viscous dominant, given that the Reynolds number for this flow component $\text{Re}_r \equiv \rho v_r L/\mu \approx 1$, wherein L is the length of the chamber. In the absence of an imposed pressure gradient, the equation governing momentum conservation of the flow in the chamber, the length of which is considerably larger than its width, then reduces to a balance between the viscous drag and the centrifugal body force acting on the fluid:

$$\mu \frac{\partial^2 v_r}{\partial y^2} \approx -\rho\omega^2 r \quad (5)$$

where y is the vertical direction spanning the depth of the chamber. The above then suggests that

$$v_r \approx -r \quad (6)$$

which, upon substitution into the dominant force balance in Equation 2 together with the scaling in Equation 4, leads to a linear relationship between the particle dimension and the position at which they concentrate:

$$r \approx -a \quad (7)$$

consistent with that observed in Figure 5f.

3. Conclusion

We have demonstrated a new class of centrifugal microfluidic lab-on-a-chip systems. To the best of our knowledge, the miniature Lab-on-a-Disc (miniLOAD) concept is the first centrifugal microfluidic platform small enough to be self-contained in a handheld device. The 10 mm discs, fabricated out of SU-8 photoresist using two-step photolithography and subsequently patterned with various channel designs, are significantly smaller (by at least one order of magnitude) than the current state of the art embodied by the Lab-on-a-CD concept. In addition, all actuation components including the power supply are sufficiently small to be integrated into a solid-state, compact device that enables portable, field use. Moreover, the actuation mechanism does not involve mechanically moving parts that are commonly subject to wear and reliability issues. In place of a laboratory bench-scale motor resembling a CD player typically used in the Lab-on-a-CD platform, we drove the disc rotation by inducing azimuthal

recirculation in a fluid drop on top of which the disc was placed using asymmetric SAW radiation from a pair of transducers patterned in an offset fashion on a piezoelectric substrate. The disc rotation, at speeds up to 1400 rpm, was then used to demonstrate valving and mixing as two examples of typical microfluidic operations alongside the ability to concentrate particle suspensions, to show that the Lab-on-a-CD functionality can be reproduced at these small scales for the development of truly miniaturized and portable devices for real-time field-use diagnostics and sensing.

Supporting Information

Supporting Information is available from the Wiley Online Library or from the author.

Acknowledgements

The authors gratefully acknowledge funding from a CSIRO Flagship Project Grant on Sensor Systems for the Analysis of Aquatic Environments. L.Y.Y. is funded through an Australian Research Fellowship granted by the Australian Research Council under Discovery Project DP0985266. J.R.F. is grateful to the Melbourne Centre for Nanofabrication (MCN) for an MCN Tech Fellowship and RMIT University for the Vice-Chancellor's Senior Research Fellowship.

- [1] G. Whitesides, *Nature* **2006**, *442*, 368–373.
- [2] L. Yeo, H.-C. Chang, P. Chan, J. Friend, *Small* **2011**, *7*, 12–48.
- [3] M. Madou, G. Kellogg, *Proc. SPIE* **1998**, *3259*, 80–93.
- [4] M. Madou, J. Zoval, G. Jia, H. Kido, J. Kim, N. Kim, *Annu. Rev. Biomed. Eng.* **2006**, *8*, 601–628.
- [5] S. Haeberle, R. Zengerle, *Lab Chip* **2007**, *7*, 1094–1110.
- [6] M. Grumann, A. Geipel, L. Riegger, R. Zengerle, J. Duce, *Lab Chip* **2005**, *5*, 560–565.
- [7] J. Duce, S. Haeberle, S. Lutz, S. Pausch, F. Stetten, R. Zengerle, *J. Micromech. Microeng.* **2007**, *17*, S103–S115.
- [8] K. Abi-Samra, L. Clime, L. Kong, R. Gorkin III, T.-H. Kim, Y.-K. Cho, M. Madou, *Microfluid. Nanofluid.* **2011**, *11*, 643–652.
- [9] Z. Noroozi, H. Kido, R. Peytavi, R. Nakajima-Sasaki, A. Jasinskas, M. Micic, P. L. Felgner, M. J. Madou, *Rev. Sci. Instrum.* **2011**, *82*, 064303.
- [10] S. Haeberle, T. Brenner, R. Zengerle, J. Duce, *Lab Chip* **2006**, *6*, 776–781.
- [11] T. Li, L. Zhang, K. M. Leung, J. Yang, *J. Micromech. Microeng.* **2010**, *20*, 105024.
- [12] C.-H. Shih, C.-H. Lu, W.-L. Yuan, W.-L. Chiang, C.-H. Lin, *Biomicrofluidics* **2011**, *5*, 013414.
- [13] L. Riegger, M. Grumann, J. Steigert, S. Lutz, C. Steinert, C. Mueller, J. Viertel, O. Prucker, J. Riuhe, R. Zengerle, J. Duce, *Biomed. Microdev.* **2007**, *9*, 795–799.
- [14] Y.-K. Cho, J.-G. Lee, J.-M. Park, B.-S. Lee, Y. Lee, C. Ko, *Lab Chip* **2007**, *7*, 565–573.
- [15] J. P. Lafleur, E. D. Salin, *J. Anal. At. Spectrom.* **2009**, *24*, 1511–1516.
- [16] D. C. Duffy, H. L. Gills, J. Lin, N. F. Sheppard, G. Kellogg, *Anal. Chem.* **1999**, *71*, 4669–4678.
- [17] J. Chen, P.-C. Huang, M.-G. Lin, *Microfluid. Nanofluid.* **2008**, *4*, 427–437.
- [18] A. LaCroix-Fralish, E. J. Templeton, E. D. Salin, C. D. Skinner, *Lab Chip* **2009**, *9*, 3151–3154.
- [19] D. Mark, S. Haeberle, S. Lutz, R. Zengerle, F. Stetten, *Proc. Transducers 2009–2009 Int. Solid-State Sensors, Actuators, Microsystems Conf.*, IEEE, New York **2009**, pp. 1230–1233.
- [20] R. Gorkin, L. Clime, M. Madou, H. Kido, *Microfluid. Nanofluid.* **2010**, *9*, 541–549.
- [21] J. Garcia-Cordero, L. Basabe-Desmonts, J. Duce, A. Ricco, *Microfluid. Nanofluid.* **2010**, *9*, 695–703.
- [22] R. Shilton, N. Glass, P. Chan, L. Yeo, J. Friend, *Appl. Phys. Lett.* **2011**, *98*, 254103.
- [23] R. Hodgson, M. Tan, L. Yeo, J. Friend, *Appl. Phys. Lett.* **2009**, *94*, 024102.
- [24] J. Friend, L. Yeo, *Rev. Mod. Phys.* **2011**, *83*, 647–706.
- [25] R. Shilton, M. Tan, L. Yeo, J. Friend, *J. Appl. Phys.* **2009**, *104*, 014910.
- [26] Y. Bourquin, J. Reboud, R. Wilson, J. M. Cooper, *Lab Chip* **2010**, *10*, 1898–1901.
- [27] Y. Bourquin, R. Wilson, Y. Zhang, J. Reboud, J. M. Cooper, *Adv. Mater.* **2011**, *12*, 1458–1462.
- [28] S.-C. Wang, Y. Lai, Y. Ben, H.-C. Chang, *Ind. Eng. Chem. Res.* **2004**, *43*, 2902–2911.
- [29] M. Gröschl, *Acustica–Acta Acustica* **1998**, *84*, 432–447.
- [30] D. Chakraborty, M. Madou, S. Chakraborty, *Lab Chip* **2011**, *17*, 2823–2826.
- [31] D. Leighton, A. Acrivos, *J. Fluid Mech.* **1987**, *181*, 415–439.

Received: October 28, 2011
 Revised: January 13, 2012
 Published online: April 10, 2012